AIAA JOURNAL
Vol. 39, No. 11, November 2001

Stability of Acoustic Wave in Two-Phase Dilute Flow with Mass Transfer

Eric Daniel* and Nicolas Thévand†
Centre National de la Recherche Scientifique, 13453 Marseille Cedex 13, France

The behavior of an acoustic wave propagating in a two-phase dilute flow is analytically and numerically investigated. The focus is on the effects of a mass transfer modeled by the so-called rapid-mixing model. An analytical solution is carried out that shows a possible unstable flow regime, which means that the magnitude of a pressure wave may be amplified under particular conditions. The neutral stability condition is mainly driven by a mass transfer number, which links the heat of phase change and the equilibrium temperature. Even the mass transfer is a simplified one and far from the actual combustion of metal particles, when the analysis is applied to aluminum particles in solid rocket motor environment, unstable flow behavior is seen at low frequencies. One-dimensional simulations of the propagation of an acoustic wave are performed, and the results recovered the theoretical ones. A simulation in a two-dimensional motor leads to an oscillatory flow, which is sustained, and the amplitude of the pressure oscillation reaches an asymptotic value. This result, obtained by solving the nonlinear coupled two-phase flow equations shows that the mass transfer might be a driven mechanism for instabilities in solid rocket motor two-phase flows.

Nomenclature

a	=	sound speed, $\sqrt{(\gamma RT)}$, m/s
C_m	=	loading mass ratio
D_p	=	particle diameter, m
$\bar{\bar{I}}_d$	=	identity tensor
L	=	heat of change phase, J/(kg · m^3)
Nu	=	Nusselt number
R	=	gas constant, J/(kg · K)
St	=	acoustic Stokes number, $\omega\tau_d$
γ	=	gas ratio of specific heats
λ	=	thermal conductivity, W/(m · K)
μ	=	dynamic viscosity, kg/(m · s)
ρ^*	=	material density of a particle, kg/m^3
τ_t, τ_d	=	thermal and dynamic relaxation time, s
ω	=	wave pulsation, 1/s
$\dot{\varpi}$	=	rate of mass transfer, kg/(m^3 · s)

Subscripts

g	=	gas phase
p	=	particulate phase

Introduction

THE propagation of an acoustic wave in a two-phase mixture with mass transfer is analytically and numerically investigated. This topic is important as evident in recent papers found in the literature.[1−3] Beyond the fundamental aspects, this subject is of prime interest in the field of combustion instability occurring in solid rocket motor (SRM) flows. The flow in such motors is due to the combustion of a solid propellant in which some metallized particles are embedded (generally aluminum particles) to increase the specific impulse. Some motors demonstrate an unstable behavior, which leads to oscillatory flows. The total effect of the particles is ambiguous. Three stages in the lifetime of the particles can be identified. These are the ignition and the agglomeration at the propellant surface, the distributed combustion (within the core flow), and the formation of oxide particles[4] (alumina in the case of initial aluminum particles). Alumina particles are inert, and it is well-known that such particles tend to damp traveling acoustic waves.[5−7] It has also been shown that the first stage is a damping mechanism because the particles at the surface propellant diminish the unsteady burning response function of the propellant at high-frequency pressure oscillations[2] (≈2000 Hz). Consequently, the combustion of the particles, or more generally a possible mass transfer between the gas and the dispersed phase, can be considered as a phenomenon that should be studied to help in the explanation of the instabilities observed at low frequencies. Nevertheless, aluminum combustion in an SRM is a very complicated process and still not well understood: It appears unlikely that with the established models that it would be possible to carry out a complete analytical study on the influence of the combustion on these instabilities. As a first approach, numerical simulations are made to predict the two-phase reactive flow,[8] but this is not sufficient to provide general physical explanations.

Several studies examined the influence of the gas–particles mass transfer on the wave propagation. Marble,[9] Davidson,[10] and Cole and Dobbins[11] supposed a mass transfer driven by Maxwell's diffusion equation. The main result is the existence of a second peak in the curve depicting the attenuation coefficient vs the acoustic Stokes number $\omega\tau_d$. The drag force and the heat transfer lead to maximum attenuation near $\omega\tau_d \approx 1$, and the second peak, associated to the mass transfer, appears around $\omega\tau_d \approx \kappa$ for very low-density ratio κ. However, no driven mechanism for a flow oscillation can be found in those studies. Dupays[2] used the so-called d^2 law for the mass transfer model. The numerical studies showed some unstable solutions that would indicate that the mass transfer might be considered as a driven mechanism.

The analysis developed here is based on a popular mass transfer model, the rapid-mixing model.[12] The difference of temperature between the gas and the particle is proportional to the mass transfer. Some previous studies[3] used this type of model, but the solutions were obtained mainly by computations, and the important role of the parameter $\bar{\varepsilon} = RT_0/L$, presented by Marble[9] as the latent heat parameter, was shown only through parametrical studies.

The different mass transfer models, Maxwell's diffusion as well as the rapid mixing model, cannot assure the reality of the combustion involved in two-phase flows in SRM. For metallized particles, most of the models assume a diffusion control process,[13] but the difference of temperature between the particles and the surrounding gas is a very important parameter. The combination of both models, diffusion and temperature dependent, can be considered as an approximation of the metal combustion. It then appears essential to study the effects of the models separately. However the aforementioned mass transfer models are just the basic mechanism of the

Received 17 November 2000; revision received 24 April 2001; accepted for publication 30 April 2001.

*Assistant Professor, Institut Universitaire des Systèmes Thermique Industriels, UMR-CNRS 6595, 5, rue Enrico Fermi. Member AIAA.

†Postdoctoral Researcher, Institut Universitaire des Systèmes Thermique Industriels, UMR-CNRS 6595, 5, rue Enrico Fermi.

aluminum particles combustion, which has very specific features: high energy released, flame around the particle with some very small alumina particles (smoke), transformation of the metal particle into an oxide particle, and possible chemical surface reactions.[14,15]

Here we propose a complete analytical solution of this problem, and we confirm the essential part of the parameter $\bar{\varepsilon}$, which we define as the mass transfer number. The dilute compressible flow equations are linearized, and solutions are found by the means of a classical modal decomposition. We will show that a neutral stability condition exists, and so some unstable flow regimes can be observed, whatever the Stokes number. Certain solutions correspond to nonphysical flow properties, but not all: The coupled aluminum particles–gaseous combustion products may lead to an unstable flow system. Also the solution presented here is important as a fundamental aspect if one considers the stability of this system of equations.

The simulation in a small motor is also presented, and the effect of the mass transfer will be evident, even for a two-dimensional calculation. This simulation is based on the solution of the governing equations in a nonlinear conservative form. The numerical solution, for expected cases extracted from the analytical solution, shows the linear development of the instability leading to a limiting cycle. The pressure amplitude reaches a maximum, and the flow oscillation is sustained by the mass transfer, the only possible driven mechanism in this case.

Governing Equations

Conservative Form

The flow is governed by the unsteady dilute two-phase compressible flow equations. The assumption of dilute two-phase flow implies that the gas and the dispersed phase are only coupled by the source terms. The volume fraction effects are negligible: No pressure terms arise in the dispersed-phase equations. It also means that the information in this phase travels via the trajectories.[16,17] The two-phase dilute flow is described by a set of partial differential equations obtained by the application of the general conservation laws (mass, momentum, and energy) in an arbitrary control volume. The system will be linearized around an equilibrium state and numerically solved in its conservative form to compare analytical and numerical results. The equations are first given in conservative form with standard notation.

Gas phase:

$$\frac{\partial \rho}{\partial t} + \nabla \cdot \rho \boldsymbol{u} = \dot{\varpi} \tag{1}$$

$$\frac{\partial \rho \boldsymbol{u}}{\partial t} + \nabla \cdot \rho \boldsymbol{u}\boldsymbol{u} + P\bar{\bar{I}}_d = \dot{\varpi}\boldsymbol{u}_p - \boldsymbol{F} \tag{2}$$

$$\frac{\partial \rho e}{\partial t} + \nabla \cdot \rho \boldsymbol{u}(e + P) = \dot{\varpi} h_p - \boldsymbol{F} \cdot \boldsymbol{u}_p - Q_{g-p} \tag{3}$$

Dispersed phase:

$$\frac{\partial \rho_p}{\partial t} + \nabla \cdot \rho_p \boldsymbol{u}_p = -\dot{\varpi} \tag{4}$$

$$\frac{\partial \rho_p \boldsymbol{u}_p}{\partial t} + \nabla \cdot \rho_p \boldsymbol{u}_p \boldsymbol{u}_p = -\dot{\varpi} \cdot \boldsymbol{u}_p + \boldsymbol{F} \tag{5}$$

$$\frac{\partial \rho_p e_p}{\partial t} + \nabla \cdot \rho_p \boldsymbol{u}_p e_p = -\dot{\varpi} h_p + Q_{g-p} \tag{6}$$

with $e = Cv_g T + \frac{1}{2}\boldsymbol{u} \cdot \boldsymbol{u}$ and $e_p = Cp_p T_p$.

This system of partial differential equations (PDE) needs closure relations that are $P = \rho RT$ (ideal gas law) and $\rho_p = N_p(\pi/6)D_p^3 \rho^*$. This last relation is only required when a mass transfer between the gas and the particles occurs, to update the diameter. To do that, the computation of the conservation equation of the number of particles per unit volume N_p is required:

$$\frac{\partial N_p}{\partial t} + \nabla \cdot \boldsymbol{u}_p N_p = 0 \tag{7}$$

This equation expresses that there is neither breakup nor coalescence of the particles.

The source terms of these equations represent the transfer between both phases (heat transfer, drag force, and mass transfer). The main purpose is to study the influence of the mass transfer on the propagation of an acoustic wave. Thus, we assume that only a simple mass transfer is necessary. The popular rapid-mixing limit model is chosen here, that is, the liquid thermal conductivity is supposed to be infinite.[12] The temperature field in the particle is uniform, but a time variation is possible. Here, this assumption is relaxed by setting the droplet temperature to be the saturation temperature.[18] Consequently, all of the heat exchanged between the gas and the particles is used for the mass transfer.[19] This is expressed by the relation

$$Q_{g-p} = \dot{\varpi} L \tag{8}$$

The heat transfer is a limiting case of convection around a spherical particle for a particulate Reynolds number $Re = (\rho|\boldsymbol{u} - \boldsymbol{u}_p|D_p)/\mu_g \to 0$ so that $Nu = 2$.

For convenience, the thermal relaxation time $\tau_t = \rho^* Cp_p D_p^2/12\lambda_g$ is introduced, and the expression of the heat transfer is then given by

$$Q_{g-p} = \rho_p Cp_p[(T - T_p)/\tau_t] \tag{9}$$

Equation (8) requires that a particle can shrink or grow according the sign of the heat transfer: In the case of a positive temperature difference, a vaporization is observed; a condensation occurs for a negative difference. Consequently, the average diameter value will remain constant, which is necessary for further linearization around an equilibrium state.

Stokes's law can be used for the drag force because the particulate Reynolds number is very small in an acoustically perturbed flow. Thus,

$$\boldsymbol{F} = \rho_p[(\boldsymbol{u} - \boldsymbol{u}_p)/\tau_d] \tag{10}$$

where τ_d is the dynamic relaxation time $\tau_d = \rho^* D_p^2/18\mu_g$.

Linearized Governing Equations

The preceding system of PDEs is linearized around an equilibrium state that is characterized by dynamic and thermal equilibrium: $u_0 = u_{p0}$ and $T_0 = T_{p0}$. Each quantity is written as the sum of a steady and unsteady part:

$$f = f_0 + f' \tag{11}$$

The equilibrium quantities are denoted by a 0 subscript, and a prime notation is related to an unsteady quantity. The following analysis is carried out only for the one-dimensional equations, in which only the first-order terms are retained. The spatial derivatives of average values are assumed to be negligible. For convenience, the prime notation is dropped, and the quantities refer to unsteady values.

Gas phase:

$$\frac{\partial \rho}{\partial t} + \rho_0 \frac{\partial u}{\partial x} + u_0 \frac{\partial \rho}{\partial x} = \dot{\varpi} \tag{12}$$

$$\rho_0 \left\{ \frac{\partial u}{\partial t} + u_0 \frac{\partial u}{\partial x} \right\} + \frac{\partial P}{\partial x} = -F \tag{13}$$

$$\rho_0 \left\{ \frac{\partial Cv_g T}{\partial t} + u_0 \frac{\partial Cv_g T}{\partial x} \right\} + P_0 \frac{\partial u}{\partial x} = \dot{\varpi}(h_{p0} - e_0) - Q_{g-p} \tag{14}$$

Dispersed phase:

$$\frac{\partial \rho_p}{\partial t} + \rho_{p0} \frac{\partial u_p}{\partial x} + u_0 \frac{\partial \rho_p}{\partial x} = -\dot{\varpi} \tag{15}$$

$$\rho_{p0} \left\{ \frac{\partial u_p}{\partial t} + u_0 \frac{\partial u_p}{\partial x} \right\} = F \tag{16}$$

$$\rho_{p0} \left\{ \frac{\partial Cp_p T_p}{\partial t} + u_0 \frac{\partial Cp_p T_p}{\partial x} \right\} = -\dot{\varpi}(h_{p0} - e_{p0}) + Q_{g-p} \tag{17}$$

and the source terms are now

$$Q_{g-p} = \rho_{p0} Cp_p[(T - T_p)/\tau_t] \tag{18}$$

$$\boldsymbol{F} = \rho_{p0}[(\boldsymbol{u} - \boldsymbol{u}_p)/\tau_d] \tag{19}$$

$$\dot{\varpi} = \rho_{p0} Cp_p[(T - T_p)/L\tau_t] \tag{20}$$

Note that the mass transfer appears only in the mass and the energy conservation equations. In both momentum equations, the term is shown to be of second order and, therefore, negligible. In the energy equations, this term is multiplied by the difference of the total enthalpy of the phase from the surface particle and the internal energy of the considered phase. We define $h_p = e_p + L$, and the term in the energy equation can be read as

$$h_{p0} - e_0 = (Cp_p - Cv_g)T_0 + L \tag{21}$$

$$h_{p0} - e_{p,0} = L \tag{22}$$

The solution of Eqs. (12–17) may be analytically obtained by assuming a decomposition of each quantity written as $f(x,t) = \hat{f} e^{iKx} e^{-i\omega t} \cdot K = k_1 + ik_2$, where K is the complex wave number and ω is the acoustic wavelength. The system is solved after the components of the wave number are known. They are obtained by calculating the determinant of this system, which must be equal to zero to ensure a nontrivial solution.

The analysis of the resulting equations shows that only the variables T, ρ, and u are independent, and the determinant of the linear system of equations is

$$\begin{vmatrix} \Omega\{1 + \gamma\beta\kappa[(1-\phi)/-i\Omega\tau_t]\} & 0 & -(\gamma-1)T_0 K \\ \Omega\kappa\rho_0[(C_{pp}/L)(1/-i\Omega\tau_t)] & -\Omega & K\rho_0 \\ KR & KRT_0/\rho_0 & -\Omega(1+\kappa/-i\Omega\tau_d) \end{vmatrix} \tag{23}$$

The following quantities are defined: $\Omega = \omega - Ku_0$, κ is the density ratio $\kappa = C_m/(1-C_m) = \rho_{p0}/\rho_0$, and $\beta = Cp_p/Cp$. The solution for the dispersed phase temperature is extracted from the linear system of equations:

$$T_p = 0 \tag{24}$$

There is no unsteady variation of the particle temperature that is consistent with the hypothesis of a fixed saturation temperature.

There is no mass transfer term in the particle velocity that has exactly the same formulation as for inert particles[7]:

$$u_p = u/(1 - i\Omega\tau_d) \tag{25}$$

The dispersed phase density is given by the following relation:

$$\frac{\rho_p}{\rho_{p0}} = \frac{K\Omega}{1 - i\Omega\tau_d} u + Cp_p \frac{1}{L} \frac{\Omega}{i\Omega\tau_t} T \tag{26}$$

In this equation, the mass transfer appears through a term containing the gas temperature variation.

General Analysis

In this part, the solution of determinant (23) is analytically studied. We assume that the mean velocity u_0 is equal to zero. It was previously shown that a nonzero mean velocity always decreases the rate of growth of a traveling wave, but remains positive.[7] There is no requirement to retain this term in the system of equations studied here. Also, u_0 is never associated with the mass transfer, but appears only in the term $\omega - Ku_0$, and this study is focused on the influence on the mass transfer. Keeping u_0 in the set of equations would lead to a fourth-order characteristic equation of Eq. (23) vs k_1 and k_2. The solution exists, but the complexity of the calculations prevents an analytical analysis.

Generally, the solution of such equation is numerically studied because its expression is very complex and not sufficiently comprehensive to be informative.[7,11] This is still true in this study. Most of the cases can be depicted by a numerical analysis, but if some analytical trends can be found, they would be very useful and would ensure that no cases are omitted (corresponding to physical or nonphysical cases). Furthermore, the point to be verified is the possible increasing of the amplitude of a traveling acoustic wave due to the mass transfer. That case would imply that the wave is unstable and that the mathematical translation is a negative value of the rate of growth k_2.

Before developing Eq. (23), the following parameters are defined:

$$\Phi = 1 + [(Cp_p - Cv_g)/L]T_0 \tag{27}$$

$$\bar{\beta} = \beta(1 - \Phi) \tag{28}$$

$$\bar{\bar{\beta}} = \bar{\beta} + \beta\bar{\varepsilon} \tag{29}$$

The three last parameters (27–29) are useful to simplify the various formulas, and they allow a general formulation of the determinant that recovered both the inert and the mass transfer formulation of the problem. The parameter $\bar{\varepsilon}$, a real positive number chosen according to the convention, was defined and used in the form $1/\bar{\varepsilon}$ by Marble.[9] In this study, we call $\bar{\varepsilon}$ the mass transfer number instead of the latent heat parameter. Its physical meaning is obvious and represents a relevant characterization of the mass transfer: Indeed, if $\bar{\varepsilon} \to \infty$, the particles are very volatile and the mass transfer should have a dominant effect ($\Leftrightarrow L \to 0$). Conversely, if $\bar{\varepsilon} \to 0$ the particles should tend to behave as inert particles ($\Leftrightarrow L \to \infty$).

Developing determinant (23) yields relation (30) in which K is the unknown:

$$K^2\left(1 + \frac{\bar{\bar{\beta}}\kappa}{\alpha - i\omega\tau_t}\right) = \left(\frac{\omega}{a_0}\right)^2 \left(1 + \frac{\kappa}{1 - i\omega\tau_d}\right)\left(1 + \frac{\gamma\bar{\beta}\kappa}{\alpha - i\omega\tau_t}\right) \tag{30}$$

Note that this formulation is formally identical to the case for inert particles: Formula (31) turns into the solution proposed by Temkin and Dobbins[6] by putting $\alpha = 1$ and $\bar{\bar{\beta}} = \bar{\beta} = \beta$. Considering the mass transfer leads to $\alpha = 0$ in Eq. (31). The solution of the linear system is obtained as soon as k_1 and k_2 are determined ($K = k_1 + ik_2$). This is achieved by extracting the real and the imaginary parts of K^2, which are given by

$$k_1^2 - k_2^2 = \left(\frac{\omega}{a_0}\right)^2 \left\{1 \Big/ \left[1 + \left(\frac{\omega\tau_t\bar{\bar{\beta}}\kappa}{\Omega_t}\right)^2\right]\right\} \left\{\left(1 + \frac{\kappa}{\Omega_d}\right) \times \left[1 + \gamma\bar{\beta}\bar{\bar{\beta}}\left(\frac{\varpi\tau_t\kappa}{\Omega_t}\right)^2\right] - \frac{\varpi^2\kappa^2\tau_t\tau_d}{\Omega_d\Omega_t}[\gamma\bar{\beta} - \bar{\bar{\beta}}]\right\} \tag{31}$$

$$2k_1k_2 = \left(\frac{\omega}{a_0}\right)^2 \left\{1 \Big/ \left[1 + \left(\frac{\omega\tau_t\bar{\bar{\beta}}\kappa}{\Omega_t}\right)^2\right]\right\} \left\{\frac{\omega\tau_d\kappa}{\Omega_d} \times \left[1 + \gamma\bar{\beta}\bar{\bar{\beta}}\left(\frac{\omega\tau_t\kappa}{\Omega_t}\right)^2\right] + \frac{\omega\tau_t\kappa}{\Omega_t}\left(1 + \frac{\kappa}{\Omega_d}\right)[\gamma\bar{\beta} - \bar{\bar{\beta}}]\right\} \tag{32}$$

with

$$\Omega_d = 1 + \omega^2\tau_d^2 \tag{33}$$

$$\Omega_t = \omega^2\tau_t^2 \tag{34}$$

A solution can be extracted by writing $k_1^2 - k_2^2 = \xi$ and $2k_1k_2 = \psi$ because k_1 is related to the velocity propagation of the wave ($k_1 = \omega/c$) and can be supposed to be positive:

$$k_1 = \sqrt{\left(\xi + \sqrt{\xi^2 + \psi^2}\right)/2} \tag{35}$$

$$k_2 = \psi/2k_1 \tag{36}$$

At this point it is clear that the analytical expressions of k_1 and k_2 would be very complex and so they are not developed, although certain numerical solutions for k_1 and k_2 are presented in a subsequent section.

It is easy to investigate the stability of the wave. Indeed, in the case of a positive value of k_2, the amplitude of the moving wave will decrease (attenuation), whereas it will be amplified for a negative value (unstable flow). It is then relevant to only study the sign of the imaginary part of K^2, which is written as

$$2k_1k_2 = (\omega/a_0)^2[f(\omega)/g(\omega)] \tag{37}$$

$$g(\omega) = 1 + (\omega\tau_t\bar{\bar{\beta}}\kappa/\Omega_t)^2 \tag{38}$$

$$f(\omega) = (\omega\tau_d\kappa/\Omega_d)\left[1 + \gamma\bar{\beta}\bar{\bar{\beta}}(\omega\tau_t\kappa/\Omega_t)^2\right] + (\omega\tau_t\kappa/\Omega_t)(1 + \kappa/\Omega_d)(\gamma\bar{\beta} - \bar{\bar{\beta}}) \tag{39}$$

The sign of Eq. (38) only depends on the function $f(\omega)$. One can introduce in Eq. (39)

$$\alpha_d = \omega\tau_d\kappa/\Omega_d \tag{40}$$

$$x_\omega = \bar{\varepsilon}\gamma\omega\tau_t\kappa/\Omega_t \tag{41}$$

Then the expression for $f(\omega)$ is

$$f(\omega) = -[\beta^2/(1-\gamma)^2](1-\beta)(1-\gamma\beta)\alpha_d x_\omega^2 - (1 + \kappa/\Omega_d)\beta^2 x_\omega + \alpha_d \tag{42}$$

where $\bar{\beta}$ and $\bar{\bar{\beta}}$ have been replaced by developing relations (28) and (29). The roots of this equation have to be found to study the sign of $f(\omega)$. The details of the calculations are not very interesting and are reported in the Appendix, and only the main results are presented here. An assumption for the density ratio κ is required to ensure the existence of real roots for $f(\omega)$, which is $\kappa \leq 1$. When the flow studied here is considered, this assumption is not very constraining because it is included in the dilute flow assumptions. For example, the mass ratio C_m of solid particle imbedded in a propellant of an SRM is always less than 0.3, this value being a very large one. The density ratio is then given by $\kappa = C_m/(1 - C_m) \approx 0.43$. With this assumption, one can show that $f(\omega)$ has two real roots $x_{\omega,1}$ and $x_{\omega,2}$, given in Appendix. The expression of the extremum of the function is denoted by x_ω^* and is given by

$$x_\omega^* = -\frac{(\gamma-1)^2(1+\kappa/\Omega_d)}{2(1-\beta)(1-\gamma\beta)\alpha_d} \tag{43}$$

The term $(1-\beta)(1-\gamma\beta)$ is very important because it determines the sign of the extremum and also the position of the roots x_ω^*. This term also points out the major role of the ratio of the specific heat β.

To summarize, the qualitative evolution of $f(\omega)$ vs x_ω is plotted in Fig. 1 in which all of the possible cases are shown, mainly according $(1-\beta)(1-\gamma\beta)$.

One notes that only positive values of x_ω define the function $f(\omega)$. Figure 1a shows the qualitative evolution of this function for $(1-\beta)(1-\gamma\beta) \succ 0$. The second root $x_{\omega,2}$ is positive, which separates the positive part of $f(\omega)$ in the range $\lfloor 0, x_{\omega,2} \rfloor$ and the otherwise negative values. The negative part corresponds to an unstable regime, for the wave motion, that appears then to be possible.

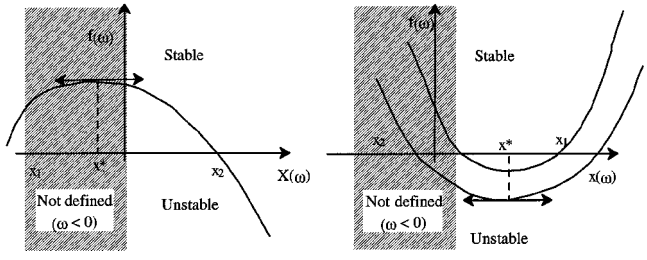

a) $(1-\beta)(1-\gamma\beta) \succ 0$: one possible configuration **b) $(1-\beta)(1-\gamma\beta) \prec 0$: two possible configurations**

Fig. 1 Stable and unstable flow regimes.

The case shown in Fig. 1a is the most expected one because the ratio β is generally greater than the unity when we consider gas–particle or gas–droplet mixtures. The calculations shown in Fig. 1a, seem to imply that the most expected case is the unstable one because the corresponding variation range of x_ω is the infinity minus $x_{\omega,2}$. However, the order of magnitude of actual x_ω is about $10^{-1}\bar{\varepsilon}$ for $\omega\tau_t \approx \omega\tau_d \approx 1$ and $\bar{\varepsilon}$ is generally less than one. Thus, for most of the physical cases, x_ω has a small value, and $f(\omega)$ can be expected to positive even though the possible unstable regime cannot be ignored.

Considering $(1-\beta)(1-\gamma\beta) \prec 0$ leads to the graphs presented in Fig. 1b. Two possible solutions appear according the sign of $x_{\omega,2}$ but whatever the solution, an unstable regime is possible. This case corresponds to less common gas–particles mixtures because of low specific heat ratios, for example, aluminum particles in SRM environments.[8]

The solution $f(\omega) = 0$ corresponds to a neutral stability condition for the spatial evolution of the wave amplitude. Even with the presence of particles, the amplitude of the wave will behave as in a pure gas phase and will remain constant [but the sound speed in the mixture is obviously different as indicated by formula (35)].

Note that an unstable behavior, meaning the growing of an acoustic wave propagation in a such medium, appears in the solution with a little restrictive condition, that is, $\kappa \leq 1$. Nevertheless, one must be aware that some but not all of these cases are physically unrealistic.

The complete solution for the sound dispersion and its attenuation from Eqs. (31) and (32) was computed in this part, confirming the earlier analysis. Some different parameters involved in the relations are here chosen arbitrarily. For example, β is chosen equal to $1/\gamma$, leading to a linear evolution of $f(\omega)$. The root of this function, which is now linear, is then unique and given by

$$x^*_{\omega,1/\gamma} = \left(\alpha_d \big/ \beta^2\right)(1 + \kappa/\Omega_d)^{-1}$$

corresponding to the neutral stability condition. This choice is motivated by the fact that this solution is a particular one, which is not included in those presented in Fig. 1. The definition of x_ω is used to extract the corresponding value of the mass transfer number:

$$\bar{\varepsilon}^*_{1/\gamma} = \gamma(\Omega_t\tau_d/\Omega_d\tau_t)(1 + \kappa/\Omega_d)^{-1}$$

One must expect that for values of $\bar{\varepsilon} \prec \bar{\varepsilon}^*_{1/\gamma}$ the flow must be stable (the sound amplitude will decrease) and be unstable otherwise, whatever the values of the Stokes number $\omega\tau_d$. The solutions are provided for three values of $\bar{\varepsilon}$, which are $\bar{\varepsilon}_S = 0.5\bar{\varepsilon}^*_{1/\gamma}$ (stable), $\bar{\varepsilon}_N = \bar{\varepsilon}^*_{1/\gamma}$ (neutral) and $\bar{\varepsilon}_U = 1.5\bar{\varepsilon}^*_{1/\gamma}$ (unstable).

The different values for the flows quantities can be chosen arbitrarily because only the unsteady values, which measure the discrepancy with the equilibrium state, are of prime interest. The density ratio κ must less than unity according the earlier condition we found, and we chose $\kappa = C_m/(1 - C_m) = 0.1765$, where $C_m = 0.15$ is a representative value of SRM loading mass ratio.

The nondimensional attenuation $\alpha_r = a_0 2k_2/\omega$ and the nondimensional dispersion $a_r = (a_0/a)^2 - 1$ is studied vs $\omega\tau_d$.

Figure 2 shows α_r for the three different values of $\bar{\varepsilon}$. Numerically, it is found that the attenuation coefficient corresponding to $\bar{\varepsilon} = \bar{\varepsilon}_N$ is identically zero ($k_2 = 0$) as predicted by relation (36). For $\bar{\varepsilon} = \bar{\varepsilon}_U$, the attenuation coefficient is negative, which means that the amplitude of an oscillation will increase when it propagates in such medium. This result is valid whatever the value of Stokes number. As it is expected, for $\bar{\varepsilon} = \bar{\varepsilon}_S$, the attenuation coefficient is positive, which is consistent with a stable behavior of a weak amplitude wave.

Those results are consistent with the definition of $\bar{\varepsilon} = RT_0/L$. Indeed, for large values of the latent heat, leading to small values of $\bar{\varepsilon}$, the particles behave as inert ones. In this case, it was proven that the dispersed phase is always a damping mechanism.

That the heat exchange between the gas and the particles is used only for the mass transfer (and consequently the particle temperature is constant) seems to be the key point to explain the possible amplification of a traveling wave.

Consider the inert case, that is, without mass transfer. The combination of the continuity equation and the energy equation of the

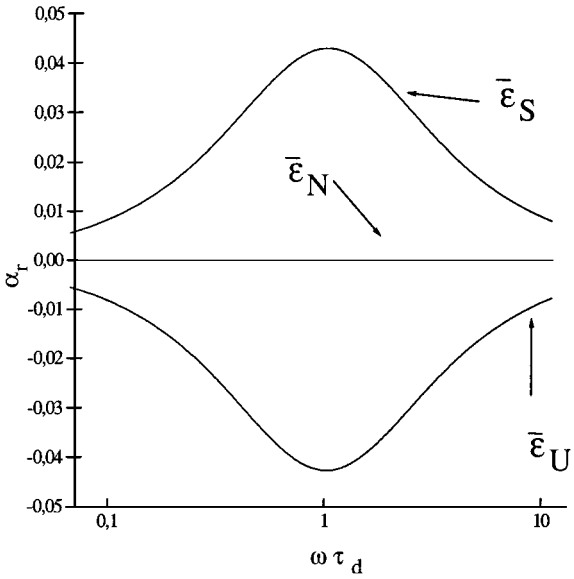

Fig. 2 Nondimensional attenuation coefficient of a two-phase flow with mass transfer.

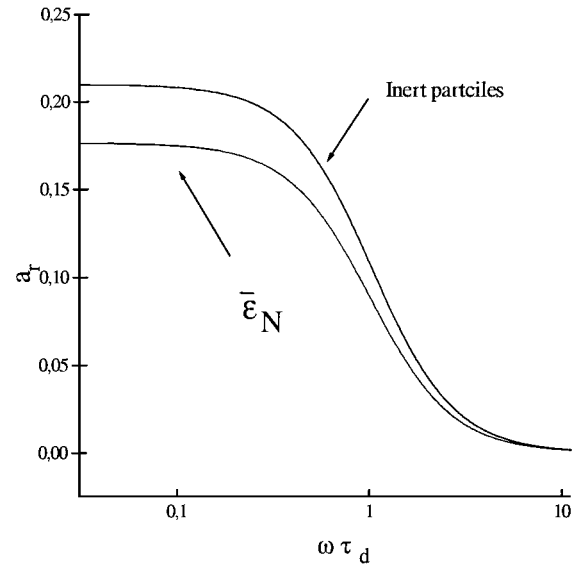

Fig. 3 Nondimensional dispersion of sound of a two-phase flow: comparison of solutions with mass transfer and inert particles.

gas phase [derived from Eqs. (12) and (14)] leads to the evolution of the gas temperature:

$$\rho_0 \frac{\partial C v_g T}{\partial t} = \frac{P_0}{\rho_0}\frac{\partial \rho}{\partial t} - Q_{g-p} = \frac{P_0}{\rho_0}\frac{\partial \rho}{\partial t} - \rho_{p0} C p_p \frac{(T - T_p)}{\tau_t} \quad (44)$$

The temperature evolution, initially due the pressure variation caused by the traveling wave, is the result of the competing effects of the time variation of the density [first source term in Eq. (44)] and the heat exchange (second source term). The heat transfer term is actually a relaxation process for the temperature, which will tend to the equilibrium one. This relaxation role is shown by writing Eq. (44) for a fixed position. The small variation assumption for all of the variables allows the term $(P_0/\rho_0)(\partial\rho/\partial t) = f'(t)$ to be written. Equation (44) is of the form $dT/dt = -aT + f'(t)$. One recognizes a dissipative term associated to the temperature in the right-hand side of this equation. The solution of this equation only gives the main tendency of the temperature evolution given by $T \equiv \mu \exp[-a(t/\tau)] + G(t)$ showing a decrease of T with time at a fixed position. Then the pressure wave amplitude, which is calculated with the equation of state $P = \rho RT$, will decrease because of the dissipative term associated with the temperature. The maximal effect is obviously observed when the characteristic time of the relaxation process and the frequency of the wave coincide, that is, when $\omega\tau_t \approx 1$. We omit the effect of the drag force in the analysis because the momentum is not affected by the mass transfer in the linearized system of equations. Also, the drag force plays the same role by relaxing the velocities.

Consider now the system when a mass transfer occurs between both phases. The combination of the continuity equation and the energy equation of the gas phase [derived from Eqs. (12) and (14)] leads to the evolution of the gas temperature:

$$\rho_0 \frac{\partial C v_g T}{\partial t} = \frac{P_0}{\rho_0}\frac{\partial \rho}{\partial t} + \bar{\varepsilon}\frac{\gamma}{\gamma - 1}(\beta - 1) Q_{g-p} = \frac{P_0}{\rho_0}\frac{\partial \rho}{\partial t}$$

$$+ \bar{\varepsilon}\frac{\gamma}{\gamma - 1}(\beta - 1)\rho_{p0} C p_p \frac{T}{\tau_t} \quad (45)$$

In the different expressions of the right-hand side of this equation, the mass transfer expression is used, then the heat transfer expression, and, eventually, T_p is set to zero as established in Eq. (24). The coefficient of this term involves the different parameters found in the present study, that is, $\bar{\varepsilon}$ and β. This formulation is very interesting compared with the inert case. The same competition between two effects (density variation and heat transfer) is still visible, and the major role of the parameter $\bar{\varepsilon}$ appears clearly in this equation. On the right hand-side, the temperature term is no longer related to a relaxation process. On the contrary, this term can make the temperature evolution diverge. When the same process is applied as for the inert case, the tendency of the solution is now of the form: $T \equiv \mu \exp[+a(t/\tau)] + G(t)$. The first term of this solution diverges. Then, because the heat term is used for the mass transfer, it does not relax the temperature toward the equilibrium state. That does not mean the temperature evolution will always diverge because the density variation may counterbalance this evolution. This competition between these two effects is driven by the values of the different coefficient of the heat flux term, mainly $\bar{\varepsilon}$. The threshold role that the parameter $\bar{\varepsilon}$ exhibits in the analytic solution of the complete system is, therefore, underlined here.

Consequently, the increase of the temperature, which is not automatically relaxed toward the equilibrium temperature because the heat transfer is used for the phase change, may drive an increase of the pressure through the equation of state. That amplifies the wave, and the system may become unstable.

In Fig. 3, a_r is plotted only for the case $\bar{\varepsilon}_N$ because the other two cases are found to be very near to this curve. It is interesting to compare this solution with the case of an inert dispersed phase, and so both solutions are plotted in Fig. 3. The evolution is qualitatively the same for both cases, but a large discrepancy is observed for low $\omega\tau_d$. When the mass transfer is accounted for, one observes that a_r tends to κ. When a fixed value of the frequency is considered, $\omega\tau_d$ varies only through the diameter value. It is not surprising to find that the major effects are mainly for low values of the diameter. The mass transfer can change considerably the diameter of the particle: For a given density ratio, the specific area $(N_p \pi D^2)$ increases as the diameter diminishes. The heat transfer (and so the mass transfer) is directly proportional to the specific area and is then more efficient for low diameters or $\omega\tau_d$. For large values of $\omega\tau_d$, the evolution of the dispersion tends to be the same and is like that in a pure gas $(a_r \approx 0)$.

Even though the solution depends on few parameters, as seen in the general expression of the determinant (23), a complete parametric study on the influence of each parameter cannot be achieved. Nevertheless, a major parameter is the density ratio κ or C_m. In previous studies,[10] it was found that a second peak exists in the attenuation curve around $\omega\tau_d \approx \kappa$ for very low κ. This peak is associated with the mass transfer, whereas the largest peak with $\omega\tau_d \approx 1$ is assumed to be due the accumulated effects of the drag and the heat transfer. We do no recover the existence of the second peak because the mass transfer is directly proportional to the heat transfer, and the effects are accumulated at the same Stokes number. We consider an unstable case, and to magnify the driven oscillatory mechanism, we chose $\varepsilon = 3\bar{\varepsilon}_N$. The influence of the density ratio is studied through

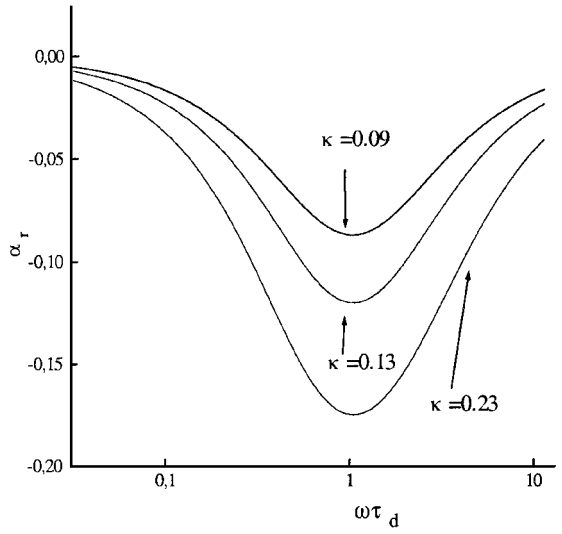

Fig. 4 Nondimensional attenuation coefficient ($\bar{\varepsilon} = 3\bar{\varepsilon}_N$): influence of the density ratio κ.

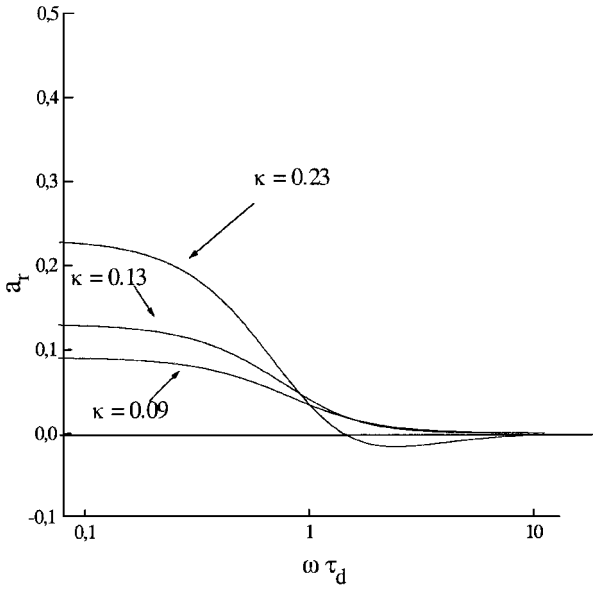

Fig. 5 Nondimensional dispersion of sound ($\bar{\varepsilon} = 3\bar{\varepsilon}_N$): influence of the density ratio κ.

three cases: $\kappa = 0.09, 0.13$, and 0.23 ($C_m = 10$, 15, and 30%, respectively). In Fig. 4, the attenuation coefficient α_r is plotted vs Stokes number for the three different values of κ.

For all of the cases, the coefficient α_r is negative, showing an unstable regime as expected. The main result shown in Fig. 4 is that the larger the loading mass ratio, the larger the amplification coefficient, which is not a surprising result. The maximum amplification is observed for $\omega\tau_d \approx 1$, whatever the density ratio.

In Fig. 5, the dispersion coefficient is displayed vs the Stokes number. Two results are prominent. The first is related to the zero limit frequency. In this case, the sound dispersion value is equal to the density ratio κ. The second result is the existence of some negative values, which means that the sound propagates faster in the two-phase mixture than in the pure gas. For large frequencies (or large particle diameters), there is no influence of the dispersed phase on the sound velocity.

This study was achieved for a fixed value of β, but the numerical solution is extracted from the general expressions of k_1 and k_2 in Eqs. (35) and (36) without any assumption. We recover results predicted by the analytical solution (for example, attenuation equal to zero), and one can, therefore, consider this one as correct.

Nevertheless, the earlier results are based on an arbitrary choice of some parameters. It is important to examine the behavior of the solution with values close to typical ones encountered in solid propellant. Aluminum particles are now supposed to undergo a mass transfer with the gas with flow properties[8] given in Table 1. The practical parameters are then $C_m = 15\%$ and $\beta = 0.48$, and in Table 1, characteritics values of required data are mentioned.

Table 1 Main thermodynamic properties for aluminum particles

Property	Value
γ	1.201
T_{p0}	2760 K
ρ^*	1766 kg/m^3
L	10.9×10^6 J/kg

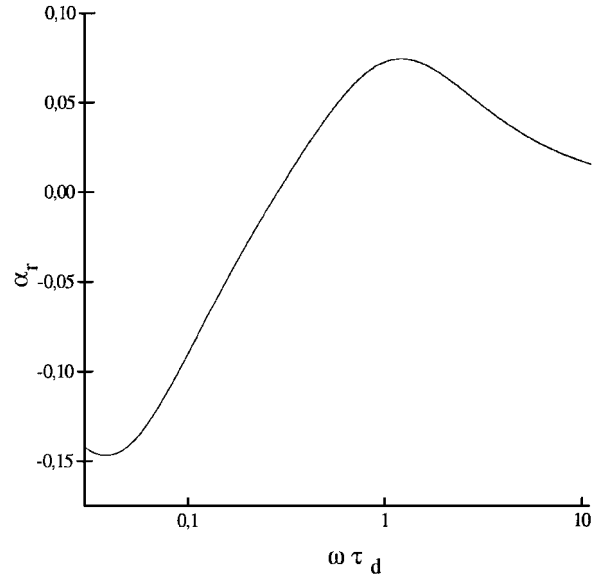

Fig. 6 Nondimensional attenuation coefficient for aluminum particles mixture.

In Fig. 6, the nondimensional attenuation coefficient vs $\omega\tau_d$ is plotted. For low Stokes number (less than 0.28), that is, for low frequency and/or low small diameter, the solution shows an unstable behavior. Above this limit, the evolution of the attenuation coefficient changes and becomes positive, which means an attenuation effect of the dispersed phase. The curve still shows one peak around the value $\omega\tau_d \approx 1$ and another one for negative values around $\omega\tau_d \approx 0.05$

In Fig. 7, the sound dispersion is plotted vs the parameter $\omega\tau_d$. Up to $\omega\tau_d \approx 0.03$, the sound velocity is larger in this medium than in a pure gas flow. Then, the dispersion becomes positive to reach a maximum value around St = 0.26. For the zero frequency limit, the result differs from the earlier one, and a_r is now different from κ. Figure 7 shows that the system of equations is very sensitive to the parameters when this case related to aluminum particles is compared to the earlier academic study. Nevertheless, for large $\omega\tau_d$ the sound velocity in the mixture is the same as in a pure gas.

Actually, thermochemical data can vary in a large range according the motor flow studied. Consequently, the pressure can be different, and doubt is possible about the values of L or β, for example. It should be interesting to examine the stability of the flow for varying frequency, independently of physical data. To do so, in Fig. 8, a three-dimensional graph shows the neutral stability condition $f(\omega) = 0$ vs Stokes number, as well as the term $\gamma\bar{\varepsilon}\kappa$. The third axis represents possible values of β. This graph is then general and exhibits possible unstable or stable flows. With the chosen data for aluminum, one observes that for low $\omega\tau_d$ an unstable regime always exists. This region also exists for large values of the frequency, but the values of $\gamma\bar{\varepsilon}\kappa$ seem not to be physical in this case.

Even though the mass transfer model was simplified, some results predicted are in agreement with other studies and expectations.[2] For

low frequency and/or low diameter, instabilities may occur in SRM flows, and the mass transfer between gas and aluminum particles may play a role that will need further investigations for actual flows, those with complex geometries, and more realistic combustion models.

Numerical Flow Simulations

The full set of PDEs in conservative form [Eqs. (1–7)] is numerically solved. Two cases are investigated. The first is related to the propagation of a wave in a one-dimensional pipe to check whether or not the numerical results of the nonlinear system are in agreement with the earlier analysis. In the second case, we simulate a two-dimensional flow in a laboratory-scale motor with a very simple geometry, a cylinder port and a nozzle. This case is interesting because the flow conditions may be slightly different than the ones required in the assumption of the stability analysis. For example, nonequilibrium (thermal and dynamic) states can be observed due to two-dimensional effects. The behavior of an acoustic wave in such a flow is discussed next.

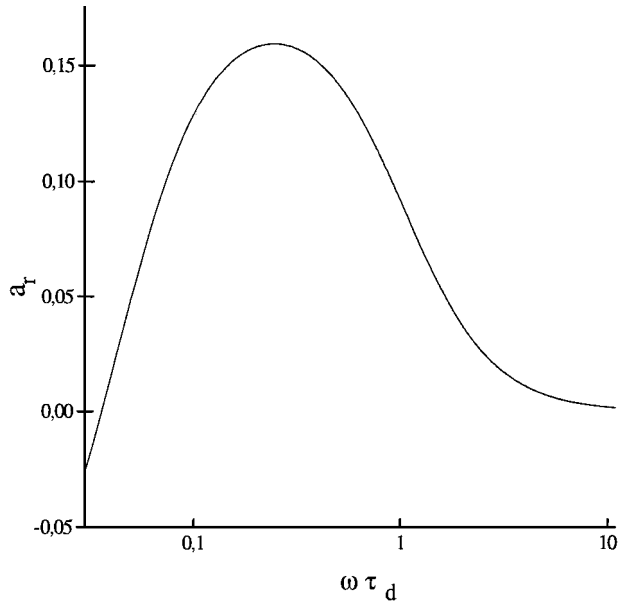

Fig. 7 Nondimensional dispersion of sound for aluminum particles mixture.

Numerical Scheme

A second order in space and time-accurate, explicit finite volume method, based on the MUSCL–Hancock methodology, is used to solve the set of equations. The numerical scheme must be a compromise between the accuracy to compute acoustic waves as well as supersonic flows encountered in the diverging part of a rocket nozzle. The numerical model has proven to compute acoustic wave properly, as well as consideration of typical compressible flows (shock waves, subsonic, supersonic flows). This was completely described in Ref. 20, and so no further details are presented.

One-Dimensional Flow

An acoustic wave propagating in a two-phase medium at rest is simulated. The mass transfer between gas and particles is included in the model. The solutions extracted by the linear stability study are expected by solving the set of conservative equations, which will illustrate the behavior of an acoustic wave in such conditions and which will also check the ability of the method to compute this kind of solution. This point is very important before solving the set of full two-phase flow equations in SRM to predict the stability in the case of more complicated flows.

The three cases described in the numerical solution section are here solved with a mass transfer number equal to $\bar{\varepsilon}_S$, $\bar{\varepsilon}_N$, and $\bar{\varepsilon}_U$, respectively. The pipe length is 20 m, which allows about 10 wavelengths to be present in the pipe. This pipe is initially filled with a gas–particles mixture at rest. At the position $x = 0$ m, the pressure is forced according a monochromatic sinusoidal law with an amplitude equal to 2% peak-to-peak of the initial pressure, and the propagation of the acoustic wave is then analyzed at a time corresponding to 10 temporal periods. The diameter of the particles is set equal to 12 μm, which is the value corresponding to the maximal attenuation in the case of inert particles.[6] The Stokes number is equal to 0.7. The pipe is divided in 500 cells in the computational domain, and the time step is restricted to a Courant–Friedrichs–Lewy number of 0.9.

In Fig. 9, a snapshot of the pressure signal in the pipe is plotted for the three cases considered. For $\bar{\varepsilon}_U$, it is clear that the wave is unstable, and the amplitude is growing while propagating in the pipe. This pressure wave can reach a large amplitude in the case of very long pipe. For $\bar{\varepsilon}_S$, the amplitude is decreasing, which corresponds to a positive attenuation coefficient. Also notice in Fig. 9 that the case for $\bar{\varepsilon}_N$ is well simulated by the finite volume scheme and that the amplitude of the signal remains constant with a high accuracy. Note

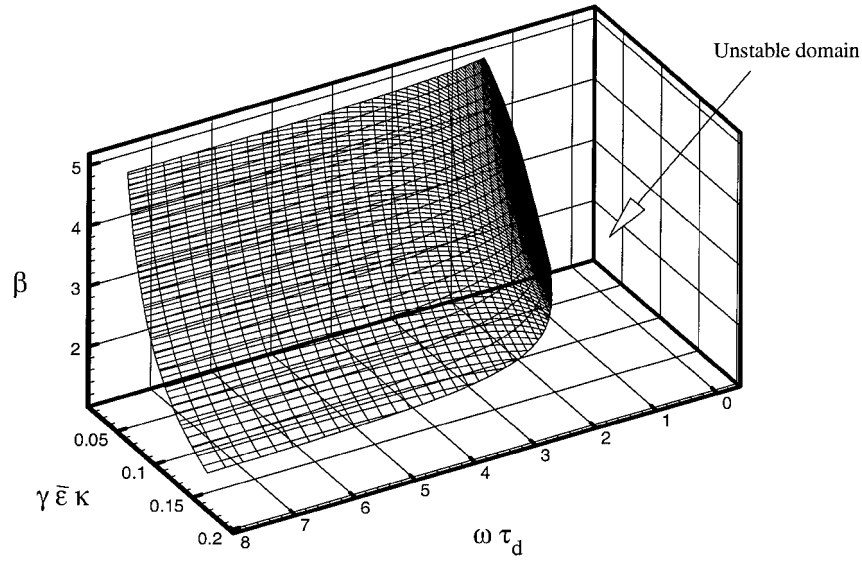

Fig. 8 Stable and unstable domains [$f(\omega) = 0$] for aluminum-gas propellant couple.

that for $\bar{\varepsilon}_U$ and $\bar{\varepsilon}_N$ there is a slight undershoot in the signal pressure around $x = 16$ m. This is due to a numerical artifact, related to the first wave entering the computational domain, which is very difficult to cancel. Consequently, the first nine wavelengths are retained for the signal analysis.

The numerical and analytical values of the nondimensional attenuation and sound dispersion are listed in Table 2.

The agreement between theoretical and numerical values is quite good, if one considers the method used here is not generally developed for acoustic studies, but for general compressible flows. The errors observed may be explained by the signal analysis method and also by the intrinsic attenuation and dispersion of the numerical scheme. A one-phase flow simulation, not presented here, showed a nondimensional attenuation coefficient equal to 3×10^{-3} and a dispersion error of about 4%.

Two-Dimensional Flow

A two-phase flow with the mass transfer in a small rocket motor is simulated. The ∇ operator in the system of equations is expressed in cylindrical coordinates. The axisymmetric motor[21] is composed of a surface injection (left-south boundary condition), a nozzle (right-south boundary condition), a wall, named head end (west boundary condition), and a symmetry axis (north boundary condition), as shown in Fig. 10. Two simulations are performed corresponding to a stable case and an unstable case according the value of the mass transfer number $\bar{\varepsilon}$. At the injection surface, the temperature and the velocity of the dispersed phase are set as the gaseous values to reach a two-dimensional steady state close to a thermal and dynamic equilibrium one.

In an actual SRM flow, the sources for acoustic energy are numerous (combustion of propellant, vortex shedding) and are not discussed here.[21–24] In the motor we simulate here, there is no acoustic source, so that a steady-state solution must be reached, free of any oscillation. When the steady-state solution is reached, the head-end pressure is forced during five wavelengths to establish a steady wave motion in the flow. Then the pressure forcing is stopped, and the time evolution of the average pressure at the west wall is analyzed. The frequency of the forcing signal is chosen to match the first longitudinal mode of the motor, which in the current calculations is equal to 2980 Hz. The amplitude is equal to 2% peak-to-peak of the average steady-state pressure in the motor (cylindrical part).

The total mass flow $\dot{m} = \dot{m}_g + \dot{m}_p$ rate is imposed at the surface injection with the following constraint: $\dot{m}_g = (1 - C_m)\dot{m}$ and $\dot{m}_p = C_m\dot{m}$ with $C_m = 15\%$. This case is interesting because the two-dimensional effects can lead to certain nonequilibrium between the gas and the particles phase. The flow is not homogeneous, and it does not totally recover the assumptions required of the analytical study. For example, in Fig. 11, the horizontal velocity components of both phases are plotted at the middle of the surface injection vs the radius. The discrepancy is not large, but it does exist.

In Fig. 12, the pressure evolution at the head-end wall are shown vs time for the stable (Fig. 12a) and the unstable (Fig. 12b) case. The forcing signal is easily seen during the five first wavelengths. In the case of the stable flow, the signal is attenuated, as expected, when the forcing is stopped. For the second case, the signal is sustained after the forcing period, and also a growth of the amplitude is observed. Then, the increase of the amplitude stops, and it is noticeable that the signal reaches an asymptotic amplitude. This behavior is out of the range of the linear theory and can only be predicted by numerical simulations.

In this simulation only the mass transfer drives the oscillatory mechanism. There is no other mechanism, such as a response at a pressure oscillation of the surface injection. This calculation shows the role that may be played by the particle in more complex flows,

Table 2 Comparison between numerical and theoretical values of nondimensional attenuation and sound dispersion coefficients

	$\bar{\varepsilon}_S$		$\bar{\varepsilon}_N$		$\bar{\varepsilon}_U$	
Values	α_r	a_r	α_r	a_r	α_r	a_r
Theoretical	0.2215	0.68	0	0.6715	−0.2197	0.6478
Numerical	0.2173	0.671	1.2×10^{-2}	0.6713	−0.198	0.598

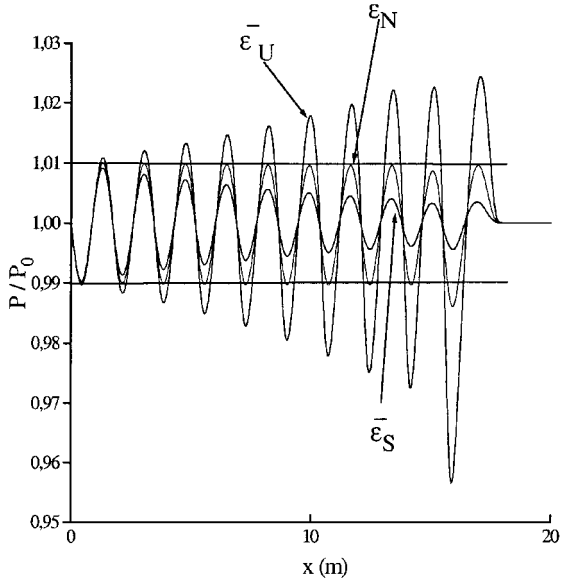

Fig. 9 Snapshot of the pressure in a pipe for three different values of $\bar{\varepsilon}$.

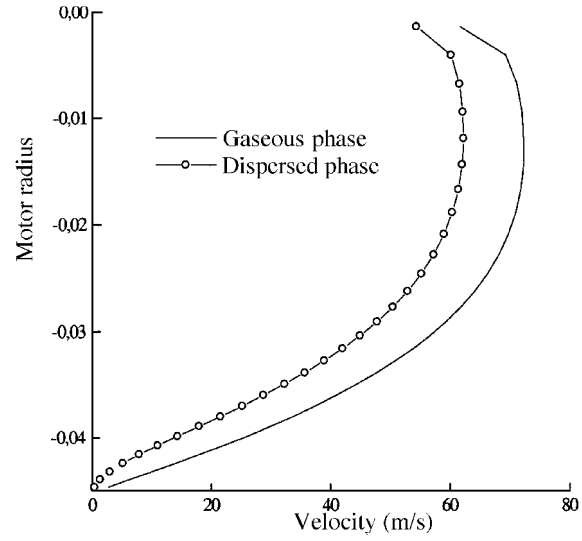

Fig. 11 Cross section of the horizontal component of the velocity vs the motor radius at the middle of the surface injection.

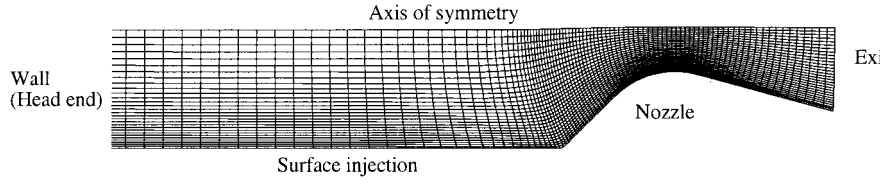

Fig. 10 Mesh (98 × 30 cells) and the boundary conditions.

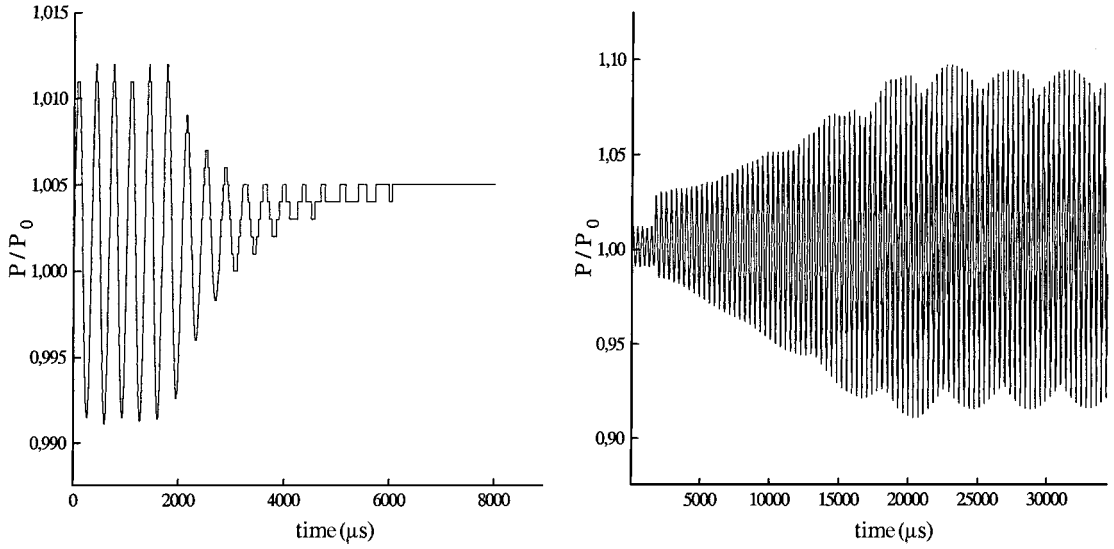

Fig. 12 Time evolution of the head-end pressure signal.

in which the level of the instabilities measured is not explained. The mass transfer model used here is very simple compared with those required for SRM, but similar phenomena may be explained by an equivalent driven mechanism based on a mass transfer.

Conclusion

An analytical solution of the linearized equations of a dilute two-phase flow including mass transfer between the gas and the particles is provided. A stability domain is extracted showing the possibility of an acoustic wave to be amplified or attenuated. The neutral stability condition is essentially dependent on the value of a nondimensional number, defined as $\bar{\varepsilon} = RT_0/L$. The mass transfer is modeled by a simple approach based on the temperature difference between both phases (gas and dispersed phase). Although the model is far from an actual mass transfer, the temperature difference is generally involved in such a process. For example, this difference is a basic parameter used to model the evaporation and combustion of aluminum particles, that is, Law's model. Nevertheless, there is a major role for the mass transfer on the stability of an acoustic wave, and at the least it is important for obtaining a complete analytical solution. We showed that the flow may become unstable, whatever the frequency or the particle diameter, or, in short, whatever the acoustic Stokes number $\mathrm{St} = \omega\tau_d$.

The analytical solution was recovered by the numerical solution of the full system of differential equations of the two-phase dilute flow. The behavior of a monochromatic acoustic wave propagating in a pipe was demonstrated. The agreement between the numerical and analytical solution was quite good. The simulation of a two-phase flow was also performed. In the case of an expected unstable flow, a limiting cycling is obtained, the amplitude of an acoustic wave being amplified and reaching an asymptotic value. This phenomenon is obviously out of the range of the linear theory and can only be predicted by numerical simulation.

Even though the mass transfer model used here was a simple one, certain instability phenomena observed might by explained thanks to a similar driven mechanism that could be more complicated considering actual SRM flows.

Appendix: Real Roots of $f(\omega)$

The expression of Eq. (42) is

$$f(\omega) = [\beta^2/(1-\gamma)^2](1-\beta)(1-\gamma\beta)\alpha_d x_\omega^2 - (1+\kappa/\Omega_d)\beta^2 x_\varpi + \alpha_d \tag{A1}$$

with $x_\varpi = \bar{\varepsilon}\gamma\omega\tau_t\kappa/\Omega_d$. The roots of this equations have to be found from the sign of $f(\omega)$. The discriminant Δ of Eq. (A1) must be positive to ensure x_ϖ is a real number. There is little difficulty to find the expression of Δ, namely,

$$\Delta = \beta^2\left\{\beta^2\left[\left(1+\frac{\kappa}{\Omega_d}\right)^2 + \gamma\left(\frac{2\alpha_d}{\gamma-1}\right)^2\right] - \beta(\gamma+1)\left(\frac{2\alpha_d}{\gamma-1}\right)^2 + \left(\frac{2\alpha_d}{\gamma-1}\right)^2\right\}$$

Note that Δ appears to be a quadratic function of β. Let Δ_Δ define the discriminant of Δ. In the case of negative values of Δ_Δ, there are no real roots for Δ, and the sign of this last function is then given by $[2\alpha_d/(\gamma-1)]^2$, that is, positive. Using this condition, we assure that x_ϖ is a real number (positive or negative), which was the first constraint to verify. When the expression of Δ_Δ is developed, a conditional relation is extracted, which is

$$\frac{\omega\tau_d}{1+(\omega\tau_d)^2} - \frac{1}{1+(\omega\tau_d)^2} \prec \frac{1}{\kappa} \tag{A2}$$

It is easy to show that, if $\kappa \leq 1$, Δ_Δ is always negative. If $\kappa \succ 1$, the last inequality depends on the value of the term $\omega\tau_d$ and both negative and positive Δ_Δ can be expected. Therefore, we now suppose that $\kappa \leq 1$ and that Eq. (A2) is always verified.

Therefore, $f(\omega)$ has two real roots $x_{\varpi,1}$ and $x_{\omega,2}$ given by

$$x_{\omega,1} = -(\gamma-1)^2\frac{(1+\kappa/\Omega_d)\beta^2 + \sqrt{\Delta}}{2\beta^2(1-\beta)(1-\gamma\beta)\alpha_d} \tag{A3}$$

$$x_{\omega,2} = -(\gamma-1)^2\frac{(1+\kappa/\Omega_d)\beta^2 - \sqrt{\Delta}}{2\beta^2(1-\beta)(1-\gamma\beta)\alpha_d} \tag{A4}$$

References

[1] Temkin, S., "Sound Propagation in Dilute Suspensions of Rigid Spheres," *Journal of the Acoustical Society of America*, Vol. 103, No. 2, 1997, pp. 838–849.

[2] Dupays, J., "Mass Transfer Effects on Sound Propagation in a Droplet-Gas Mixture," 5th International Symposium on Special Topics in Chemical Propulsion, Stresa, Italy, June 2000.

[3] Daniel, E., Lee, M. G., Murphy, J., and Krier., H., "Numerical Analysis of the Stability of Solid Rocket Motors: Two-Phase Flows Aspects," AIAA Paper 2000-0312, Jan. 2000.

[4] Price, E. W., "Combustion of Metalized Propellants," *Fundamentals of Solid Propellants Combustion*, Vol. 90, Progress in Astronautics and Aeronautics, AIAA, New York, 1984, pp. 479–513.

[5] Culick, F. E. C., "The Stability of Three Dimensional Motions in Combustion Chamber," *Combustion Sciences and Technology*, Vol. 10, 1975, pp. 109–124.

[6] Temkin, S., and Dobbins, R. A., "Attenuation and Dispersion of Sound by Particulate-Relaxation Processes," *Journal of the Acoustical Society of America*, Vol. 40, No. 2, 1966, pp. 317–324.

[7]Basset, T., Daniel, E., and Loraud, J. C., "Analytical and Numerical Results on the Attenuation and Dispersion of an Acoustic Wave Through a Two-Phase Flow," *International Journal of Numerical Methods for Heat and Fluid Flows*, Vol. 7, No. 7, 1997, pp. 722–736.

[8]Daniel, E., "Eulerian Approach for Two-Phase Reactive Solid Rockets Flows with Aluminum," *Journal of Propulsion and Power*, Vol. 16, No. 2, 2000, pp. 309–317.

[9]Marble, F. E., "Some Gas Dynamic Problems in the Flow of Condensing Vapors," *Astronautica Acta*, Vol. 14, 1969, pp. 585–614.

[10]Davidson, G. A., "Sound Propagation in Fogs," *Journal of the Atmospheric Sciences*, Vol. 32, 1975, pp. 2201–2205.

[11]Cole, J. E., and Dobbins, R. A., "Propagation of Sound Through Atmospheric Fog," *Journal of the Atmospheric Sciences*, Vol. 27, No. 4, 1970, pp. 426–434.

[12]Sirignano, W. A., "Fuel Droplet Vaporization and Spray Combustion Theory," *Progress in Energy and Combustion Science*, Vol. 9, 1983, pp.291–322.

[13]Law, C. K., "A Simplified Theoretical Model for the Vapor-Phase Combustion of Metal Particles," *Combustion Science and Technology*, Vol. 7, 1973, pp. 197–212.

[14]Brooks, K. P., and Beckstead, M. W., "Dynamics of Aluminum Combustion," *Journal of Propulsion and Power*, Vol. 11, No. 4, 1995, pp. 769–780.

[15]Dreizin, E. L., "Experimental Study of Stages in Aluminum Particle Combustion in Air," *Combustion and Flame*, No. 105, 1996, pp. 541–556.

[16]Daniel, E., Saurel, R., Larini, M., and Loraud, J. C., "A Multiphase Formulation for Two-Phase Flows," *International Journal of Numerical Methods for Heat and Fluid Flow*, Vol. 4, 1994, pp. 269–280.

[17]Ishii, R., Umeda, Y., and Yuhi, M., "Numerical Analysis of Gas-Particle Two-Phase Flows," *Journal of Fluid Mechanics*, Vol. 203, 1989, pp. 475–515.

[18]Faeth, G. M., "Current Status of Droplet and Liquid Combustion," *Progress in Energy and Combustion Science*, Vol. 3, 1977, pp. 191–224.

[19]Crowe, C., Sommerfeld, M., and Tsuji, Y., *Multiphase Flows with Droplets and Particles*, CRC Press, Boca Raton, FL, 1998, Chap. 4.

[20]Thevand, N., Daniel, E., and Loraud, J. C., "On High-Resolution Schemes for Solving Unsteady Compressible Two-Phase Dilute Flows," *International Journal for Numerical Methods in Fluids*, Vol. 31, 1999, pp. 681–702.

[21]Lupoglazoff, N., and Vuillot, F., "Simulation Numérique Bidimensionnelle des Ecoulements Instationnaires dans les Propulseurs à Propergol Solide," *La Recherche Aérospatiale*, No. 2, March–April 1992, pp. 21–41.

[22]Kuentzmann, P., "Instabilités de Combustion," AGARD Lecture Ser. 180, Sept. 1991.

[23]Blomshield, F. S., Crump, J. E., Mathes, H. B., Stalnaker, R. A., and Beckstead, M. W., "Stability Testing of Full-Scale Tactical Motors," *Journal of Propulsion and Power*, Vol. 13, No. 3, 1997, pp. 349–355.

[24]Vuillot, F., Basset, T., Dupays, J., Daniel, E., and Lupoglazoff, N., "Two-Dimensional Navier–Stokes Stability Computation for Solid Rocket Motors: Rotational, Combustion and Two-Phase Flow Effects," AIAA Paper 97-3326, July 1997.

J. P. Gore
Associate Editor